



Neuro-intelligent networks for Bouc–Wen hysteresis model for piezostage actuator

Sidra Naz^{1,a}, Muhammad Asif Zahoor Raja^{2,b} , Ammara Mehmood^{3,4,c},
Aneela Zameer^{5,d}, Muhammad Shoaib^{6,e}

¹ Department of Electrical Engineering, Pakistan Institute of Engineering and Applied Sciences, Nilore, Islamabad 45650, Pakistan

² Future Technology Research Center, National Yunlin University of Science and Technology, 123 University Road, Section 3, Douliou, Yunlin 64002, Taiwan, ROC

³ School of Electrical and Electronic Engineering, The University of Adelaide, Adelaide, Australia

⁴ Present Address: School of Electronics Engineering, Kyungpook National University, Daegu, South Korea

⁵ Department of Computer and Information Sciences, Pakistan Institute of Engineering and Applied Sciences, Nilore, Islamabad 45650, Pakistan

⁶ Department of Mathematics, COMSATS University Islamabad, Attock Campus, Attock 43600, Pakistan

Received: 5 January 2021 / Accepted: 30 March 2021

© The Author(s), under exclusive licence to Società Italiana di Fisica and Springer-Verlag GmbH Germany, part of Springer Nature 2021

Abstract Piezoelectric stage has become promising actuator for wide applications of micro-/nano-positioning systems represented mathematically with Bouc–Wen hysteresis model to examine the efficiency. In this investigation, the numerical study of piezostage actuator based on nonlinear Bouc–Wen hysteresis model is presented by neurocomputing intelligence via Levenberg–Marquardt backpropagated neural networks (LMB-NNs). Numerical computing strength of Adams method is implemented to generate a dataset of LMB-NNs for training, testing and validation process based on different scenarios of input voltage signals to piezostage actuator model. The performance of LMB-NNs of nano-positioning system model is validated through accuracy measures on means square error, histogram illustrations and regression analysis.

List of symbols

b	Network bias
c	Damping coefficient
d	Output displacement
e	Error between actual and desired outputs
f	Nonlinear function
h	Hysteresis response

^a e-mail: sidranaz_19@pieas.edu.pk

^b e-mail: rajamaz@yuntect.edu.tw (corresponding author)

^c e-mail: ammara.mehmood@adelaide.edu.au

^d e-mail: aneela@pieas.edu.pk

^e e-mail: dr.shoaib@cuiatk.edu.pk

I	Identity matrix
J	Jacobian matrix
k	Stiffness coefficient
LMB	Levenberg–Marquardt backpropagation
m	Mass of sliding object
MSE	Mean square error
N	Hidden layers neurons
NN	Neural networks
p	Downhill step
Q	Step interval
R	Regression value
T	Time variable
W	Weight matrix
X	Input voltage
Z	Number of sample data points
α, β, γ	Hysteresis loop shape control parameters
Δ	Piezoelectric coefficient
λ	Nonnegative scalars of identity matrix

1 Introduction

Piezoelectric stage (PS) is an electromechanical device which produces motion in one degree of freedom and is operated by piezoceramic actuators (PCAs). These piezoceramic actuators have well positional accuracy with sub-nanometer resolution, highly stable with large blocking force and fast response with in milliseconds; therefore, they are extensively used in the applications of micro- or nano-positioning systems like space antenna applications [1], lithography systems [2], sensors applications [3], energy harvesting [4], micromechanical systems [5] and micro-robotics [6]. The PCAs produced nonlinearity into a PS system because of hysteresis and piezoceramic polarization, while hysteresis is the response for the input voltage with output displacement that highly destroy the positional accuracy of PS systems [7, 8]. Therefore, in nano-positioning applications, the hysteresis must be suppressed for high accuracy. Hence, precise modeling is still the challenging task for researchers. In order to cancel out the nonlinear hysteresis effect, an inverse compensation is introduced to the PS system. The nonlinear hysteresis model is categorized as operator-based hysteresis model [9] and differential systems-based hysteresis model [10]. The common model of differential systems used to explain the hysteresis of PS contains the Duhem model [11], Backlash model [12] and Bouc–Wen model [13]. The operator-based hysteresis model contains Prandtl–Ishlinskii model, [14] Krasnosel’skii–Pokrovkii model, [15] and Preisach model [16].

The recent, relevant, reported studies for electro-vibro dynamic hysteresis modeling of piezostage actuator (PSA) in different applications include a feedforward control methodology of dynamic hysteresis inverse classic Preisach model [17], and proportional-integral-derivative control [18] is proposed for PSA. Interval type-2 fuzzy system based on gradient optimization is presented for hysteresis modeling and feedforward control of the PSA [19]. The design of hysteresis by autoregressive exogenous neural network for is presented in order to enhance the performance accuracy of PSA for vibrations of helicopter vibrations [20]. Another approach for hysteresis compensation based on adaptive control of single neuron is proposed to dynamically control the PSA input by utilizing the combination of supervised learning and Hebb learning rules [21]. A self-tuning neural network control approach

is offered to apprehend the system accuracy by tracking PSA uncertainties and nonlinear hysteresis [22]. A slide mode controller based on Prandtl-Ishlinskii model is introduced [23]. Another dynamic delay Prandtl-Ishlinskii model is presented to characterize the dynamic and asymmetrical features of PSA in order to suppress the hysteresis effect [24]. Lee et al. presented finite-time integral terminal sliding mode and time-delayed estimation approaches in order to achieve fast, accurate, and robust force tracking performance [25]. The Elman neural network-based dynamic hysteretic operator is used to alter the multi-valued mappings of hysteresis [26]. A polynomial-based disturbance fractional-order model is presented to describe the intricate PSA hysteresis effect that considerably suppressed hysteresis nonlinearity over a wide bandwidth [27]. A tracking control Pneumatic muscle PSA is presented, based on echo state Gaussian process and nonlinear predictive control model for lower limb exoskeleton [28]. Moreover, the recurrent neural network-based inversion model is introduced to compensate the nonlinearities of PSA in order to get a high-accuracy, broadband and less computational complexity [29].

1.1 Related study

Different researchers present different approaches in order to optimize the system parameters of this nonlinear effect of input and output displacements. The particle swarm optimization (PSO) method is used to optimize the nonlinearity of Dahl model, Duhem model, generalized Duhem and Bouc-Wen hysteresis models [11]. The parameter identification of Duhem model is employed by genetic algorithm as well as clonal selection algorithm [30]. For Bouc-Wen hysteresis model accuracy, the least square method has also been used [31]. Transitional Markov chain Monte Carlo approach is exploited to optimize the parameters of Bouc-Wen model [32]. Improved artificial bee colony algorithm is presented in order to identify hysteresis parameters [33]. Furthermore, the optimization of nonlinear effect of piezo actuator for Bouc-Wen hysteresis model has been performed by hybrid adaptive differential evolution [34]. Hence, the Bouc-Wen hysteresis model is commonly adaptive technique to model the hysteresis of PS systems as only one auxiliary differential system is essential to explain the behavior of hysteresis.

Numerical methods focused on soft computing paradigm are commonly used to solve various problems of differential systems [35, 36]. Some recently published studies of paramount significance contain solution of mathematical model for Painlevé-II representing the dynamics of nonlinear optics [37], nonlinear Bratu's equation arising in electrically conducting solid models [38, 39], reactive transport system of soft tissue [40], Van-der-Pol oscillatory nonlinear systems [41, 42], convergent/convergent fluidic flow systems [43, 44], thin-film flow studies [45, 46], combustion theory [47], nonlinear circuit theory models [48, 49], astrophysics [50], mathematical models involving Carbon nanotubes [51], heartbeat dynamic models [52], dusty plasma [53], HIV infection spread models [54], atomic physics [55, 56], piezoelectric transducer modeling [57], wind power [58, 59], load dispatch problem [60], financial models [61, 62], nonlinear fractional dynamic modeling with Riccati fractional differential equations (FrDEs) [63, 64] and Bagley-Torvik FrDEs [65].

1.2 System model: Bouc-Wen model for hysteresis modeling of piezoelectric actuator

The nano-position moving stage excited by piezo actuator (PA) is graphically demonstrated in Fig. 1. By applying an input voltage x on the piezoelectric stack, the elongation is formed in the stack due to piezoelectric effect, which exerts force on the sliding mass m and caused essential displacement d . The unsymmetrical relationship between this output displacement

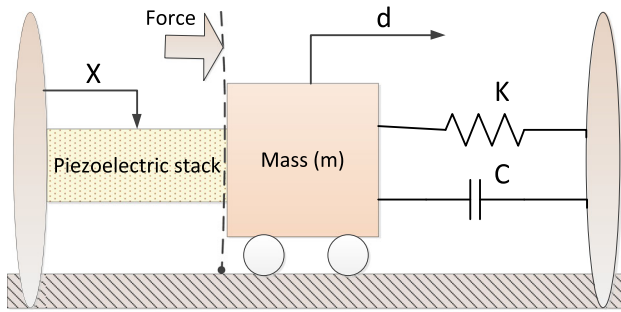


Fig. 1 System model

Table 1 Piezo actuator settings

Parameter	Value
C	$6.4665 \times 10^3 \text{ Ns/m}$
k	$1.7333 \times 10^6 \text{ N/m}$
m	0.4763
n	1
δ	$2.4825 \times 10^{-5} \text{ m/v}$
α	0.5011
β	0.7017
γ	0.9997

and applied voltage is the hysteresis loop that can be described by Bouc-Wen model. The standard Bouc-Wen model (BWM) is first presented by Bouc in 1967 [66] where the hysterical act of external applied force and output displacement is numerically expressed in form of function; then, in 1976 the generalized version of this function is proposed by Wen. This model comprises of two equations, the nonlinear first-order state equation and the linear output equation of input and state signals. It can be demonstrated in numerous variety of hysteresis behavior depending on the selection of parameters. The electromechanical expression for dynamic hysteresis model of piezo actuator can be described in Eqs. (1) and (2).

$$m \ddot{d}(t) + c \dot{d}(t) + k d(t) = k(\delta x(t) - h(t)), \tag{1}$$

$$\begin{aligned} \dot{h}(t) = & \alpha \dot{x}(t) - \beta |\dot{x}(t)| |h(t)| |h(t)|^{n-1} \\ & - \gamma \dot{x}(t) |h(t)|^n, \end{aligned} \tag{2}$$

where x signifies the input voltage, d is the output displacement, t indicates time variable, c is the damping coefficient, h denotes hysteresis, k represents stiffness coefficient and δ symbolize the piezoelectric coefficient. The parameters α , β , γ and n are the magnitude and shape control variables of hysteresis, where α, β and γ control the basic shape, while order n is responsible for the sharpness and smoothness of the hysteresis loop that switch the response from elastic to plastic. The values of all these model parameters are given in Table 1.

1.3 Problem statement and significance

The enriched importance of piezoelectric actuator attracts different researchers to implement numerous techniques to observe the dynamics of system, but the soft computing technique has not been exhaustively examined for the analysis of Bouc–Wen hysteresis model. The main objective of this investigation is to exploit soft computing paradigm through the ability of Levenberg–Marquardt backpropagated neural networks (LMB-NNs) to solve the differential system representing in Eqs. (1–2). The proposed LMB-NNs can be a good alternative to be exploited for Duhem model, Dahl model and Prandtl–Ishlinskii model.

1.4 Contribution and innovative insights

The creative elements of the designed computing infrastructure are briefly illustrated as:

- Novel application of neuro-heuristic technique based on Levenberg–Marquardt backpropagated neural networks (LMB-NNs) is presented to study the Bouc–Wen hysteresis model for piezostage actuator.
- The dataset of Bouc–Wen hysteresis model is created by exploiting the strength of Adam numerical solver for training, testing and validation purpose.
- The efficacy of the scheme is validated by variation in applied input voltage signals to piezostage actuator model on accuracy through performance metrics based on mean squared error, error histogram illustrations, as well as regression analyses.
- Apart from the proven competence of precise solution, other valued key characteristics of the scheme are sound procedures, smooth execution, fast steady convergence, reliability and extensibility.

1.5 Organization

The rest of the paper is organized as follows: Sect. 2 narrates methodology based on supervised neural network employed for solving the hysteresis modeling of piezoelectric actuator. In Sect. 3, outcomes with necessary interpretation are narrated, while concluding inferences are listed in Sect. 4.

2 Methodology

In this section, the methodology is presented that consists of the three parts. Initially, the creation of data set by Adams numerical method, then formulation of LMB-NNs and finally the performance indices is discussed. The graphical abstract of design methodology is represented in Fig. 2. The steps of our proposed work are demonstrated in algorithms 1.

2.1 Adams numerical method

Adams numerical approach for first-order system is written as:

$$\frac{dy}{dx} = f(x, y), \quad (3)$$

$$Y_{l+1} = y_l + \int_{t_l}^{t_{l+1}} \frac{dy}{dx} dt = y_l + \int_{t_l}^{t_{l+1}} f(y, t) dt, \quad (4)$$

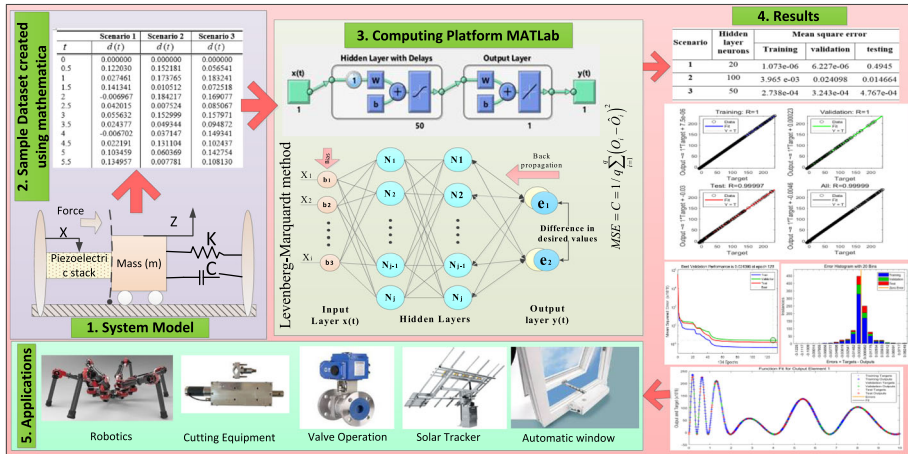


Fig. 2 Graphical abstract of proposed methodology

where y signifies output of linear first-order ordinary differential equation, x represents the input value, Y_{l+1} symbolize the first-order interpolation iterative approach, and t denotes the time interval.

Adams methods are based on the principle of approximating the integral within the interval (t_l, t_{l+1}) with a polynomial. There are two kinds of Adams methods, the explicit and the implicit types. The Adams–Bashforth (AB) methods are called the explicit type, and the Adams–Moulton (AM) methods are called the implicit type. The AB and AM methods of the first order are essentially the methods of forward and backward Euler. The second-order versions of these methods are very common (obtained by using a linear interpolant). In Eq. (5), the second-order Adams–Bashforth (AB2) method is described.

$$Y_{l+1} = y_l + \frac{q}{2}(3f(y_l, t_l) - f(y_{l-1}, t_{l-1})) \tag{5}$$

where q is the step interval. The Adams–Moulton second order (AM2) is an implicit method, also referred to as the trapezoidal principle given below:

$$Y_{l+1} = y_l + \frac{q}{2}(f(y_{l+1}, t_{l+1}) + f(y_l, t_l)) \tag{6}$$

2.2 Levenberg–Marquardt backpropagation method

In 1944, Kenneth Levenberg and Donald Marquardt developed the Levenberg–Marquardt algorithm, that exploits the strength of steepest decent method (SDM) and the Gauss–Newton method (GNM). Due to the hereditary convergent efficiency of GNM and of SDM stability, the algorithm is robust. The minimum function $F(x)$ is initially determined in the LM algorithm as:

$$F(x) = \sum_{i=1}^l \left(\frac{(f_i(x))^2}{2} \right), \tag{7}$$

while J represents Jacobian of the function and the LM method proceed as:

$$(J_a^T J_a + \lambda_a I) p_a = -J_a^T f_a, \tag{8}$$

where λ_i represents positive scalar values, I stands for identity matrix, and p is downhill step. The updated rule for weights in LBM-NNs algorithm is given as:

$$w_{a+1} = w_a - (J_a^T J_a + \lambda_a I)^{-1} J_a e_a, \tag{9}$$

Here e_a and w_a are error and weight vector, respectively.

The convergence rate of the LM algorithm is higher than both GNM and SDM. LM algorithms have two feasible alternatives for the path of the algorithm at each iteration. At the same time, it can handle several parameters.

Algorithms 1:

```

Part 1:
Create dataset for three input signals for t= 0:10 with step size0.1 in Mathematica
Input: Train data  $D_{train}$ , Test data  $D_{test}$ ,  $n_i$  ( $i = 1, 2, \dots, k$ )
Output: Mean Square error, regression analysis, error histogram, training states, fitting curve

Begin FFNNs
// Define problem\
Output i.e.,  $y(t) = f(x(t-1), \dots, x(t-d), y(t-1), \dots, y(t-d))$ 
Signal input values i.e.,  $X(t)$ 
Target time series i.e.,  $Y(t)$ 
//Initialization of parameters
Training i.e., 70%
Validation i.e., 15%
testing i.e., 15%,
No of hidden neurons  $N_i$ 
No of delays  $\omega$ 
//load training data building neural network
Net = fitnet( $N_i$ );
//apply feedforward propagation
net = feedforward net(10);
net = train(net,x,t);
y = net(x);
perf = perform(net,y,t);
//if error is greater than minimum error than
//apply backward propagation and update weights

Repeat
For all  $(x_i, y_j) \in$  Dataset do
    Compute  $y_j$ 
    Compute  $\delta_{ci}$ 
    Compute  $w_{ji}, v_{kj}$ 
End For

End

//Training Network using LM Method
Perform initialization of the weights;
While not stop-criteria do
    Determine  $e^r(w)$  for each entry;
     $e1 = \sum_{r=1}^r e^r(w)^t e^r(w)$ ;
    calculate  $j^r(w)$  for each entry;
    Repeation
        Determine  $\Delta w$ ;
         $E2 = \sum_{r=1}^r e^r(w + \Delta w)^t e^r(w + \Delta w)$ ;
        If ( $e1 \leq e2$ ) then
             $\mu = \mu * \zeta$ ;
        endif;
    until ( $e2 < e1$ )
         $\mu = \mu / \zeta$ ;
         $w = w + \Delta w$ ;
end while;
    
```

Artificial neural networks are composed of a series of linked units called artificial neurons. A signal can be transmitted to another neuron through each synapse between neurons. The state of neurons can easily be expressed by entries generally real number between [0, 1]. Neurons are usually arranged into layers' structure with different types of transformation functions. On their inputs, different layers can perform different types of transformations. In this methodology, 20 to 100 hidden layers were used in order to achieve the desire output. The basic structure of proposed neural network is shown in Fig. 3. Here, a Levenberg–Marquardt

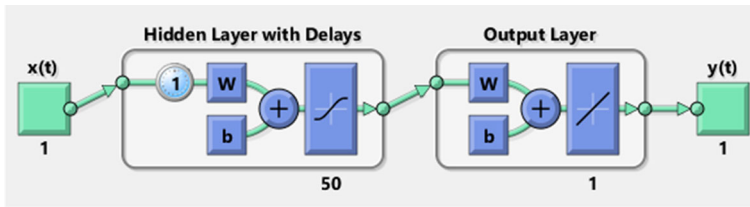


Fig. 3 Structure of supervised neural network

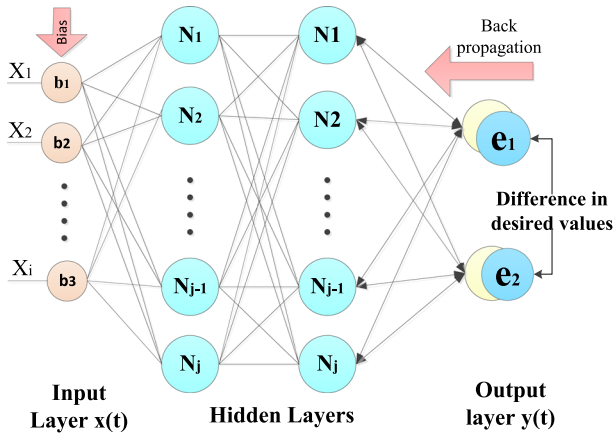


Fig. 4 Levenberg–Marquardt backpropagation

backpropagation algorithm-based neural network is presented to optimize the Bouc–Wen hysteresis model of piezostage actuator graphically shown in Fig. 4.

2.3 Performance indices

The performance of our proposed work has been illustrated by regression analysis, error histogram, curve fitting and mean square error.

2.3.1 Regression analysis

Regression analysis is a powerful form of statistics that help to analyze the relationship of interest between two or more variables. Although there are several forms of regression analysis, they all analyze the effect of independent variables over dependent variables. It is most commonly used for forecasting and prediction, where its application overlaps greatly with the field of machine learning. The regression method helps to confidently decide which variables matter most, the relationship between these variables and which variable can be ignored. Regression model shows that Y_i is a function of X_i and ζ , with e_i which represents a random statistical noise as given in Eq. (10).

$$Y_i = f(X_i, \zeta) + e_i. \tag{10}$$

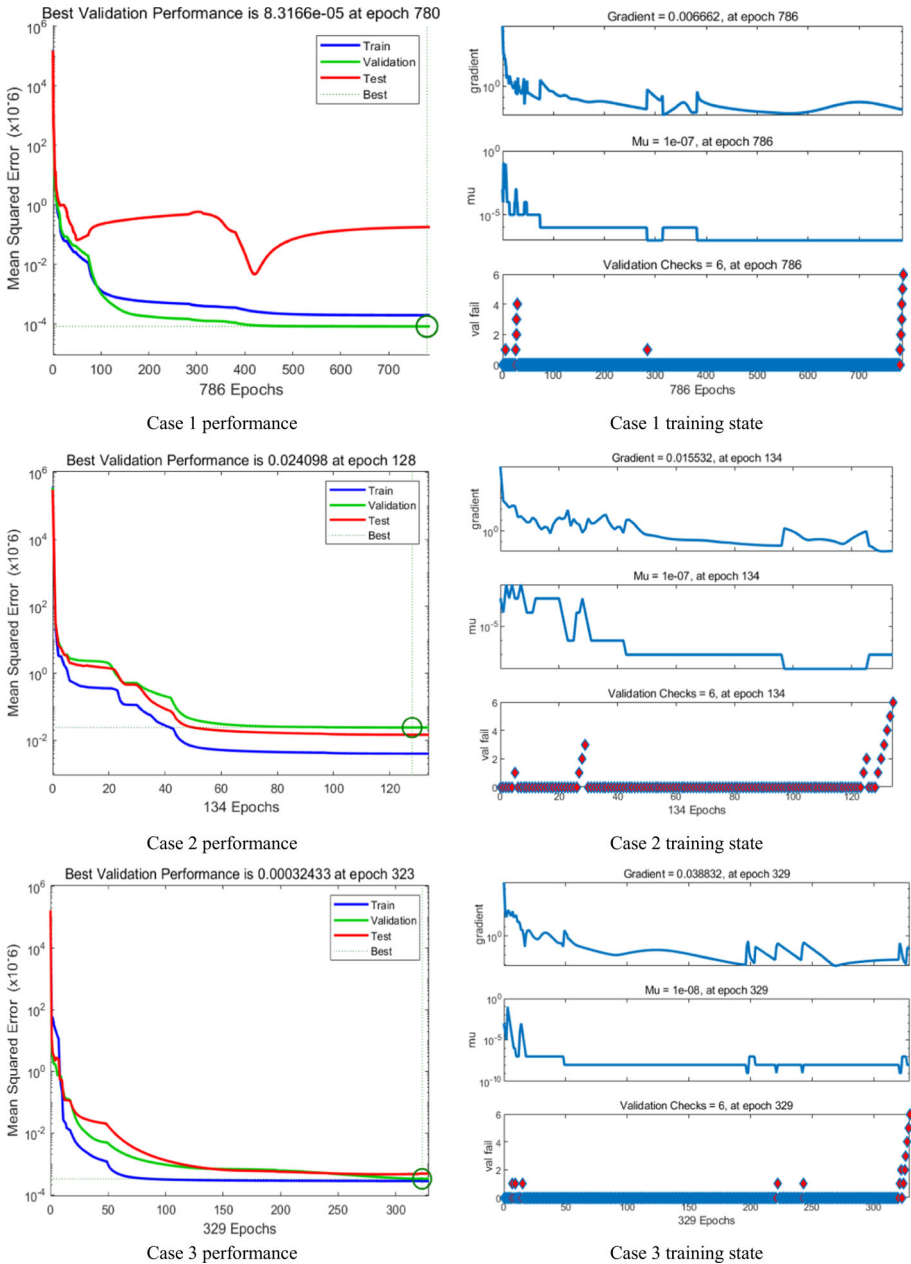


Fig. 5 Comparison of performance and training states of input signals

2.3.2 Error histogram

Error histogram shows the differences between predicted values and targeted values obtained after training a feedforward deep neural network. Since these error values show how expected

Table 2 Datasets of displacement (mm) for all three scenarios

t	Case 1 $d(t)$	Case 2 $d(t)$	Case 3 $d(t)$
0.0	0.000000	0.000000	0.000000
0.5	0.122030	0.152181	0.056541
1.0	0.027461	0.173765	0.183241
1.5	0.141341	0.010512	0.072518
2.0	-0.006967	0.184217	0.169077
2.5	0.042015	0.007524	0.085067
3.0	0.055632	0.152999	0.157971
3.5	0.024377	0.049344	0.094872
4.0	-0.006702	0.037147	0.149341
4.5	0.022191	0.131104	0.102437
5.0	0.103459	0.060369	0.142754
5.5	0.134957	0.007781	0.108130
6.0	0.069603	0.047261	0.137877
6.5	-0.001124	0.094198	0.112305
7.0	0.010395	0.090301	0.134320
7.5	0.072201	0.060561	0.115327
8.0	0.103859	0.027865	0.131761
8.5	0.079369	0.011089	0.117513
9.0	0.031153	0.007300	0.129875
9.5	-0.001778	0.008679	0.119109
10	-0.005499	0.010753	0.128487

values vary from the target values, they may also be negative. Bins represent the vertical bars on the graph, and y -axis denotes number samples from given dataset. Zero line on graph corresponds to the zero error.

2.3.3 Mean square error

The mean square error (MSE) of an estimator is used in statistics to calculate the average error squares, i.e., the average square difference between the expected values and the real value. It can be used as a loss function in order to analyze the model performance. The mathematical expression of MSE is shown in Eq. (11).

$$\text{MSE} = \frac{1}{s} \sum_{i=1}^s (Y_i - \hat{Y}_i)^2, \quad (11)$$

where s is the number of sample data points, Y and \hat{Y} are true output and estimated output. The error can be obtained from the difference of estimated and true output values.

3 Results and discussion

In this section, dynamic hysteresis model of piezo actuator using proposed LBM-NNs is presented with numerical and graphical illustrations of outcomes. Results are presented for

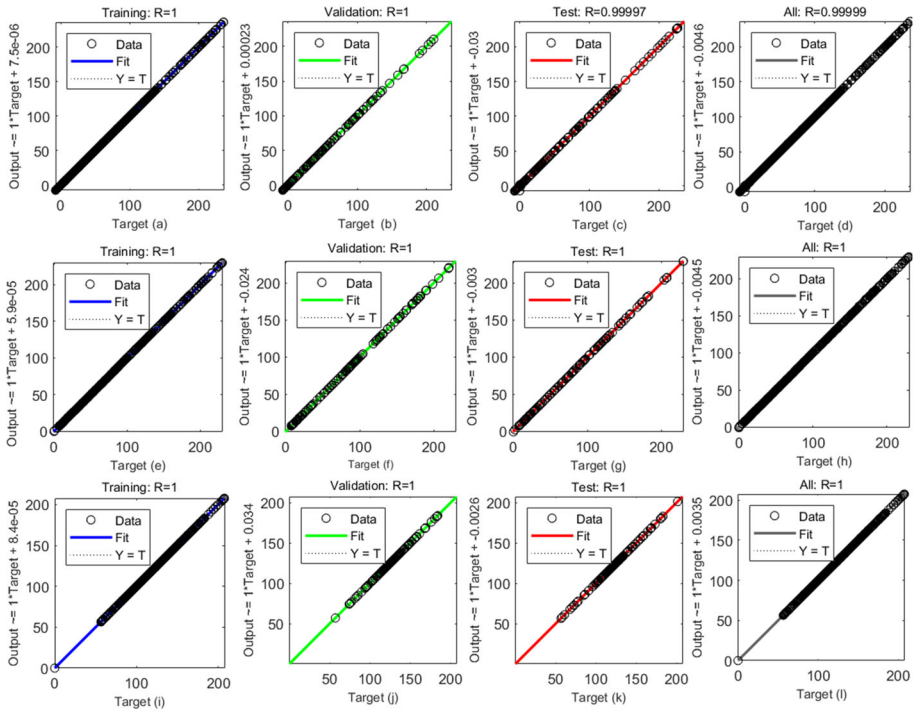


Fig. 6 Regression Analysis of training, testing and validation for all scenarios

all three cases of dynamic hysteresis model of piezo actuator by variation of input voltage signal as per following details.

The solution of dynamic hysteresis model of piezo stage actuator is presented by taking following three cases:

3.1 Case 1: piezoelectric actuator model with type 1 input

In this case study, dynamics of Bouc-Wen hysteresis model is represented in Eqs. (1) and (2) for piezostage actuator with given initial conditions presented by choosing type 1 input voltage signal in $t \in [0, 10]$. The initial conditions are:

$$d(0) = 0, \quad d'(0) = 0, \quad h(0) = 0.$$

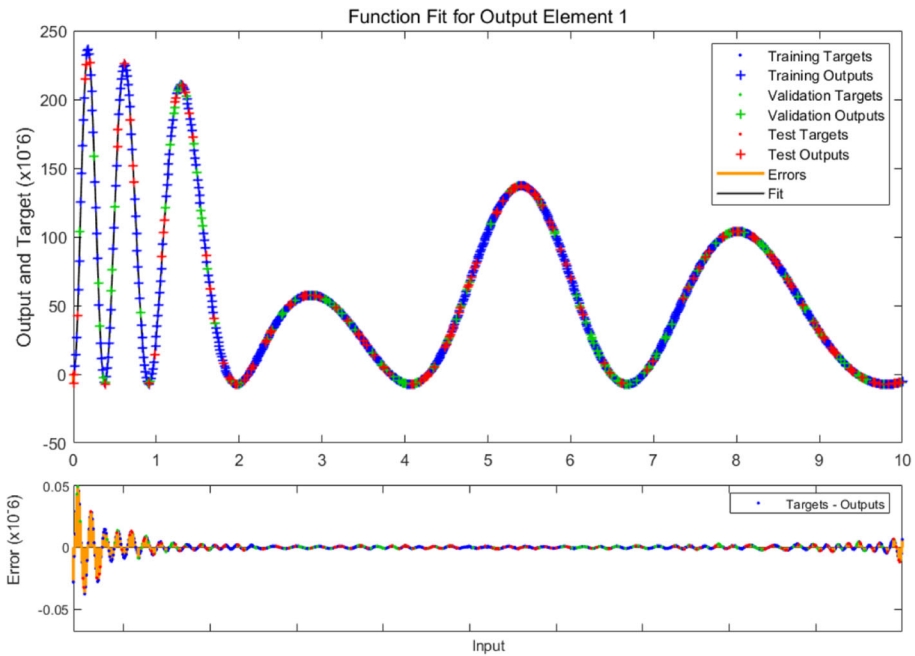
The type 1 input voltage signal is shown in Eq. (12).

$$x(t) = 5e^{-0.1t} (\sin(6\pi te^{-0.346t} - 1.5) + 1), \tag{12}$$

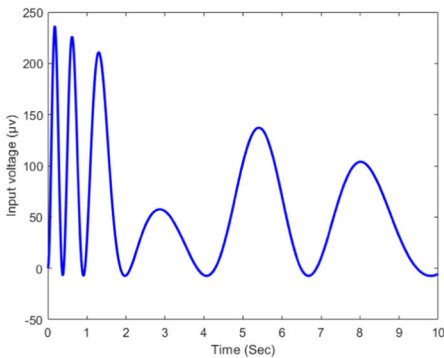
Using Eq. (12), the updated Bouc-Wen hysteresis model for piezoelectric actuator is given in Eqs. (13–14).

$$\begin{pmatrix} m\ddot{d}(t) + c\dot{d}(t) + kd(t) + kh(t) \\ -5\delta ke^{-0.1t} (\sin(6\pi te^{-0.346t} - 1.5) + 1) \end{pmatrix} = 0, \tag{13}$$

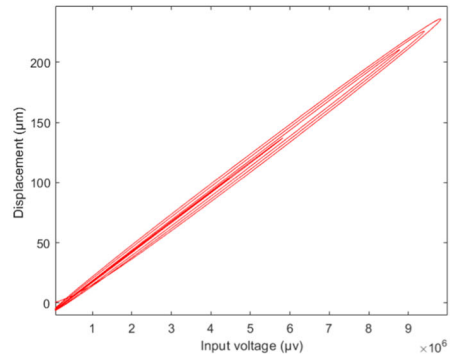
$$\dot{h}(t) = (\alpha\delta - \gamma|h(t)|^n) \begin{pmatrix} -5e^{-0.1t} (-6\pi e^{-0.346t} + 6.522te^{-0.346t}) \\ \cos(1.5 - 6\pi te^{-0.346t}) - 0.5e^{-0.1t} (1 - \sin(1.5 - 6\pi te^{-0.346t})) \end{pmatrix}$$



(a) Output displacement and model error curve fitting



(b) input signal



(c) hysteresis loop

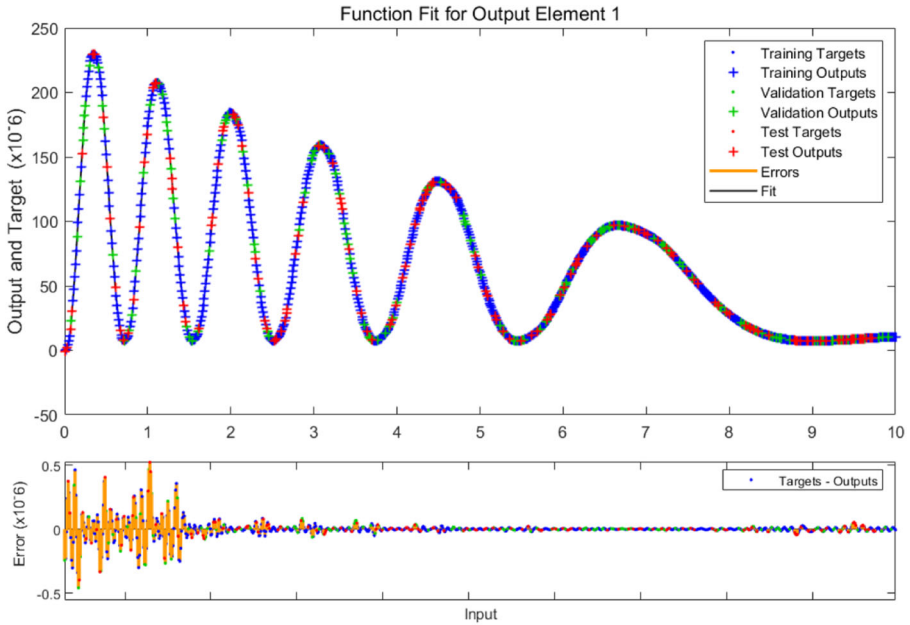
Fig. 7 Case 1: curve fitting: a output displacement curve fitting, b input signal 1, c hysteresis loop

$$-\beta \left| -5e^{-0.1t} \begin{pmatrix} -6\pi e^{-0.346t} \\ +6.522te^{-0.346t} \end{pmatrix} \cos \begin{pmatrix} 1.5 \\ -6\pi te^{-0.346t} \end{pmatrix} - 0.5e^{-0.1t} \left(1 - \sin \begin{pmatrix} 1.5 \\ -6\pi te^{-0.346t} \end{pmatrix} \right) \right| h(t)|h(t)|^{n-1}. \tag{14}$$

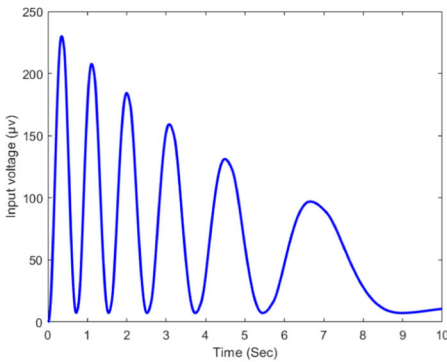
3.2 Case 2: Piezoelectric actuator model with type 2 input

In this case study, a type 2 input voltage signal for time $t \in [0, 10]$ is shown in Eq. (15) chosen for the dynamic of BWM of piezoelectric actuator described in Eqs. (16–17).

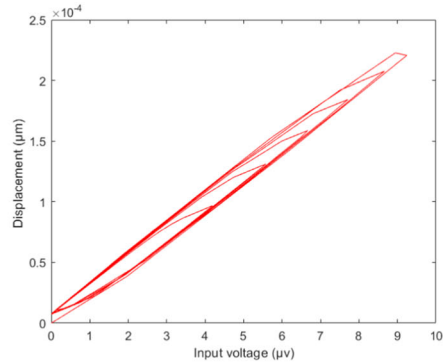
$$x(t) = 5e^{-0.13t} (\cos(3\pi te^{-0.09t} - 3.15) + 1), \tag{15}$$



(a) Output displacement and model error curve fitting



(b) Input signal 2

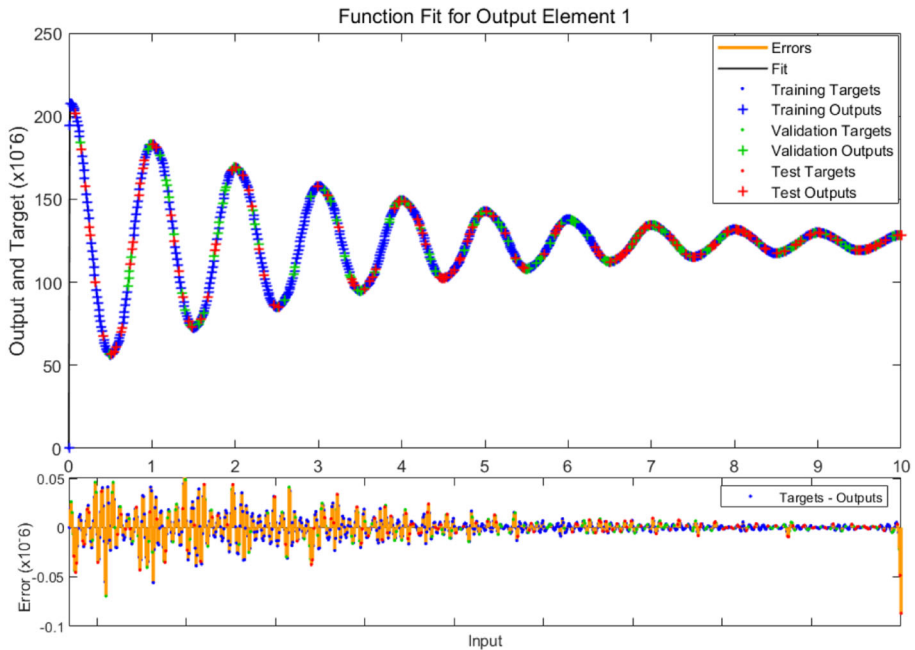


(c) Hysteresis loop

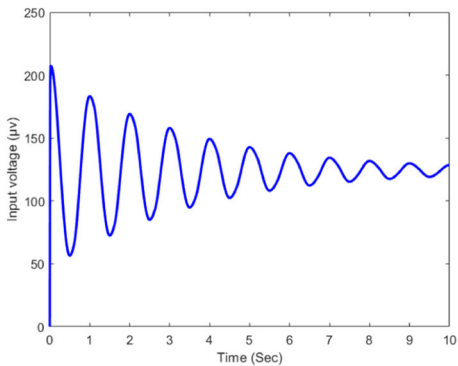
Fig. 8 Case 2: curve fitting a output displacement curve fitting, b input signal 2, c hysteresis loop

$$\left(\begin{aligned} & m\ddot{d}(t) + c\dot{d}(t) + kd(t) + kh(t) \\ & -5\delta ke^{-0.13t} (\cos(3\pi te^{-0.09t} - 3.15) + 1) \end{aligned} \right) = 0, \tag{16}$$

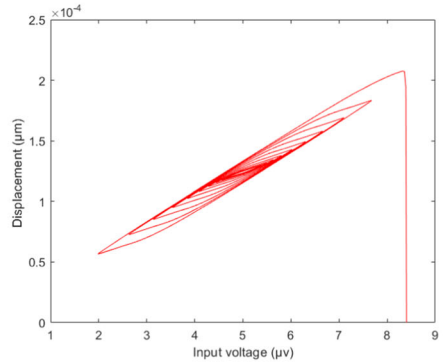
$$\begin{aligned} \dot{h}(t) = & (\alpha\delta - \gamma|h(t)|^n) \left(\begin{aligned} & -0.65e^{-0.13t} \left(\begin{aligned} & 1 + \cos(3.15 - 3e^{-0.09t}\pi t) \\ & -5e^{-0.13t} \left(\begin{aligned} & -3e^{-0.09t}\pi \\ & +0.84823e^{-0.09t}t \end{aligned} \right) \sin(3.15 - 3e^{-0.09t}\pi t) \end{aligned} \right) \end{aligned} \right) \\ & -\beta \left| -0.65e^{-0.13t} \left(1 + \cos\left(\frac{3.15 -}{3e^{-0.09t}\pi t} \right) \right) - 5e^{-0.13t} \left(\begin{aligned} & -3e^{-0.09t}\pi + \\ & 0.84823e^{-0.09t}t \end{aligned} \right) \sin\left(\frac{3.15 -}{3e^{-0.09t}\pi t} \right) \right| h(t)|h(t)|^{n-1}. \end{aligned} \tag{17}$$



(a) Output displacement curve fitting



(b) Input signal 3



(c) Hysteresis loop

Fig. 9 Case 3: **a** Output displacement curve fitting, **b** input signal, **c** hysteresis loop

3.3 Case 3: Piezoelectric actuator model with type 3 input

In this case study, a type 3 signal in $t \in [0, 10]$ shown in Eq. (18) is selected as an input signal of piezoelectric actuator in order to determine the dynamics of Bouc-Wen hysteresis model.

$$x(t) = 5 + 3.4e^{-0.24t} (\cos 2\pi t), \tag{18}$$

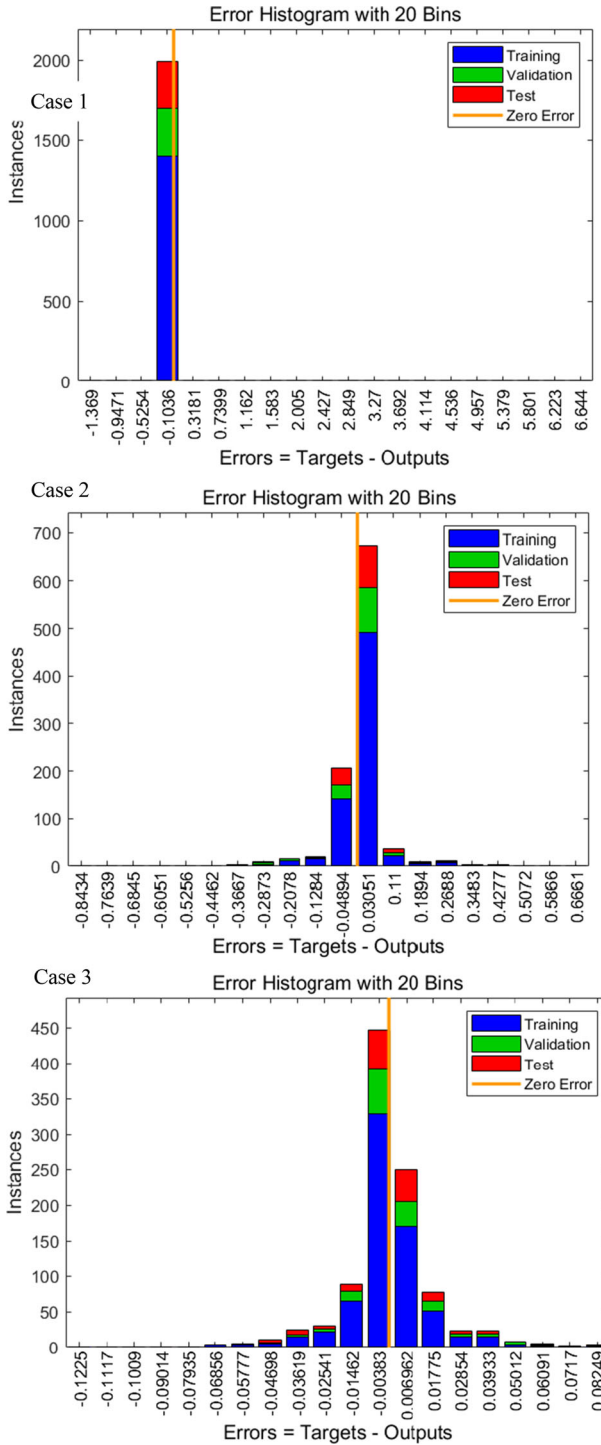


Fig. 10 Error histogram for all three cases

Table 3 Performance analysis for all three cases of proposed piezo actuator model

Case	Hidden layer neurons	Mean square error			Performance	Gradient	Mu	Epoch
		Training	Validation	Testing				
1	20	1.073e-06	6.227e-06	0.4945	8.3166E-05	6.66E-03	1.0E-07	786
2	100	3.965e-03	0.024098	0.014664	0.024098	0.015532	1.0E-07	134
3	50	2.738e-04	3.243e-04	4.767e-04	3.2433E-04	0.038832	1.0E-08	329

Now Eqs. (1) and (2) turn in the form of Eqs. (19–20).

$$\begin{pmatrix} m\ddot{d}(t) + c\dot{d}(t) + kd(t) + kh(t) \\ -5\delta k + 3.4e^{-0.24t}k\delta(\cos 2\pi t) \end{pmatrix} = 0, \tag{19}$$

$$\dot{h}(t) = \begin{pmatrix} \alpha\delta - \\ \gamma|h(t)|^n \end{pmatrix} \begin{pmatrix} -21.3628e^{-0.24t} \sin(2\pi t) \\ -0.816e^{-0.24t} \cos(2\pi t) \end{pmatrix} - \beta \begin{vmatrix} -21.3628e^{-0.24t} \sin(2\pi t) \\ -0.816e^{-0.24t} \cos(2\pi t) \end{vmatrix} |h(t)|h(t)|^{n-1}. \tag{20}$$

Initially, the dataset for all three cases was created with Adams numerical method by using ‘NDSolver’ in Mathematica platform. Different datasets for each analysis were created with step size 0.1 in order to find the solution of dynamic Bouc-Wen hysteresis model with supervised neural network. The datasets for all three cases with different input signals for selected twenty points with step size 0.5 are numerically represented in Table 2. The number of data points created for each case is 101 with step size 0.1. Furthermore, these datasets were imported into MATLAB for implementation of SNN where 90% of data points is used for training the model, 5% is for testing, and leftover 5% is used for validation purpose of obtained results. Performance analysis for all three cases of proposed dynamic hysteresis model of piezo actuator are numerically shown in Table 2, where the hidden layer neurons were kept 20, 50 and 100 according to achieve better performance. The best observed performance value for case 1 is 8.3166E-05 in 786th epoch, for case 2 is 0.024098 in 134th epoch and for case 3 is 3.2433E-04 in 329th epoch. The values of step size (Mu), gradient and mean square error (MSE) are also shown in table. To verify the model accuracy, the MSE is used that has shown optimal values for all three cases. The MSE values of training, testing and validation of proposed model for case 1 are 1.073e-06, 0.4945 and 6.227e-06, respectively. The case 3 shows minimum MSE value for testing of system that is 4.767e-04 with step size (Mu) of 1.0E-08 in 329th epoch as compared to other two cases.

The obtained results are also graphically shown in form of performance analysis, regression analysis of training, testing and validation, curve fitting of output displacement and model error and histogram. The performance analysis of dynamic hysteresis piezo actuator for all three cases is graphically illustrate in Fig. 5 where the MSE values are plot against each epoch for training, validation and testing of model. The best MSE value is achieved at case 1 for validation that is 8.31E-05 at 786 epoch. The gradient, Mu and validation check at 786 epochs are also graphically shown. The best line for case 1 is observed near 10⁻⁴, for case 2 is around 10⁻² and for case 3 is closed to 10⁻³. These graphs show that for all cases the accurate MSE value is taken; however, a bit degradation in performance of model for testing and validation is observed due to un-biasness, while the training provides best values in all graphs although during validation and testing process the target at input were not defined. The algorithm stability is shown by state estimation due to Mu. The state

estimation of proposed model is actually the step size (μ), gradient and validation check at each epoch shown in Fig. 5; here, the gradient is used to find another vector at each epoch during training. The μ represents the step size of used algorithm, and the term validation check is generalized measure of the model. The convergence results for smaller μ of all three cases are shown by these graphs; however, the best convergence is observed in case 3 where the μ value is $1\text{E}-08$ at 329 epoch.

The regression analysis of dynamic hysteresis piezo stage actuator for training, testing and validation are graphically demonstrated in Fig. 6; here, the prediction and forecasting are graphically demonstrated. It shows that the value of regression (R) is achieved approximately 1 for all three cases, which determines the closed correlation between the targets and the output vectors.

In order to find accuracy of dynamic hysteresis model of piezo actuator, the fitness graphs are plotted. And hence the error of all three cases is found. Input signals, model hysteresis, training states of fitness graphs and errors of dynamic hysteresis piezo stage model for case 1 are shown in Fig. 7, that of case 2 are shown in Fig. 8 and that of case 3 are shown in Fig. 9, respectively.

Further analysis is performed through histogram where the error is plot verses instances for all data points including training, testing and validation with 20 bins. The histogram for all three case is shown in Fig. 10. Most data points are observed to converge toward a zero error line with less extreme values. On the left side of the target line, the negative error is plotted, while the positive error is plotted on the right side. In case 1, the targeted zero error line occurred at -0.1 where it falls into the bin; in case 2, the zero error falls into the bin at 0.035 , and in case 3, the zero error line lies at -0.003 on error axis (Table 3).

4 Conclusion

In this research work, an neurocomputing heuristics is presented to model differential equations of nonlinear Bouc-Wen hysteresis model and optimized with the LMB-NNs. The dataset of piezostage actuator is created by Adams numerical method. Various experiments based on variation of input voltage signal for actuation of piezostage actuator model are conducted in order to validate, train and test the system. A neural networks approach for nonlinear hysteresis modeling of piezoelectric actuator has exposed remarkable, efficient and stable results with highest accuracy in terms of mean squared error, regression analyses and error histogram. The best testing result is obtained in case 3 where the MSE value is $4.767\text{e}-04$. The best performance is $8.3166\text{E}-05$ which is achieved by case 1 with step size $1.0\text{E}-07$ in 786 epochs. The minimum error is shown by case 3 where the zero error line lies on -0.004 .

The proposed neurocomputing intelligence algorithm can be a good alternative to be implemented on renewed applications in broad fields [67–73].

Declarations

Conflict of interest All the authors of the manuscript declared that there is no conflict of interest.

References

1. S. Shao, Y. Shao, S. Song, M. Xu, X. Ma, Structure and controller design of a piezo-driven orientation stage for space antenna pointing. *Mech. Syst. Signal Process.* **138**, 106525 (2020)
2. J. Jung, K. Huh, Simulation tool design for the two-axis nano stage of lithography systems. *Mechatronics* **20**(5), 574–581 (2010)
3. J. Joseph, S.G. Singh, S.R.K. Vanjari, Leveraging innate piezoelectricity of ultra-smooth silk thin films for flexible and wearable sensor applications. *IEEE Sens. J.* **17**(24), 8306–8313 (2017)
4. C.R. Bowen, H.A. Kim, P.M. Weaver, S. Dunn, Piezoelectric and ferroelectric materials and structures for energy harvesting applications. *Energy Environ. Sci.* **7**(1), 25–44 (2014)
5. C.H. Nguyen, U. Hanke, E. Halvorsen, Actuation of piezoelectric layered beams with d_{31} and d_{33} coupling. *IEEE Trans. Ultrason. Ferroelectr. Freq. Control* **65**(5), 815–827 (2018)
6. B. Ghosh, R.K. Jain, S. Majumder, S.S. Roy, S. Mukhopadhyay, Experimental performance evaluation of smart bimorph piezoelectric actuator and its application in micro robotics. *Microsyst. Technol.* **23**(10), 4619–4635 (2017)
7. Y. Shan, K.K. Leang, Accounting for hysteresis in repetitive control design: nanopositioning example. *Automatica* **48**(8), 1751–1758 (2012)
8. G.Y. Gu, L.M. Zhu, C.Y. Su, Modeling and compensation of asymmetric hysteresis nonlinearity for piezoceramic actuators with a modified Prandtl–Ishlinskii model. *IEEE Trans. Industr. Electron.* **61**(3), 1583–1595 (2013)
9. M.A. Krasnoselskii, A.V. Pokrovskii, *Systems with Hysteresis* (Springer, Berlin, 2012).
10. A. Visintin, *Differential Models of Hysteresis*, vol. 111 (Springer, Berlin, 2013).
11. C.J. Lin, P.T. Lin, Tracking control of a biaxial piezo-actuated positioning stage using generalized Duhem model. *Comput. Math. Appl.* **64**(5), 766–787 (2012)
12. R. Liu, X. Gao, Neural network identification and sliding mode control for hysteresis nonlinear system with backlash-like model. *Complexity* (2019).
13. W. Zhu, X.T. Rui, Hysteresis modeling and displacement control of piezoelectric actuators with the frequency-dependent behavior using a generalized Bouc–Wen model. *Precis. Eng.* **43**, 299–307 (2016)
14. A. Esbrook, X. Tan, H.K. Khalil, Control of systems with hysteresis via servocompensation and its application to nanopositioning. *IEEE Trans. Control Syst. Technol.* **21**(3), 725–738 (2012)
15. W.S. Galinaitis, Two Methods for Modeling Scalar Hysteresis and Their Use in Controlling Actuators with Hysteresis. Doctoral dissertation, Virginia Tech (1999)
16. H. Hu, R.B. Mrad, On the classical Preisach model for hysteresis in piezoceramic actuators. *Mechatronics* **13**(2), 85–94 (2003)
17. J. Chen, G. Peng, H. Hu, J. Ning, Dynamic hysteresis model and control methodology for force output using piezoelectric actuator driving. *IEEE Access* **8**, 205136–205147 (2020)
18. C. Napole, O. Barambones, I. Calvo, J. Velasco, Feedforward compensation analysis of piezoelectric actuators using artificial neural networks with conventional PID controller and single-neuron PID based on Hebb learning rules. *Energies* **13**(15), 3929 (2020)
19. P.Z. Li, D.F. Zhang, J.Y. Hu, B. Lennox, F. Arvin, Hysteresis modelling and feedforward control of piezoelectric actuator based on simplified interval Type-2 fuzzy system. *Sensors* **20**(9), 2587 (2020)
20. D. Meng, P. Xia, K. Lang, E.C. Smith, C.D. Rahn, Neural network based hysteresis compensation of piezoelectric stack actuator driven active control of helicopter vibration. *Sensors Actuators A* **302**, 111809 (2020)
21. Y. Qin, H. Duan, Single-Neuron adaptive hysteresis compensation of piezoelectric actuator based on hebb learning rules. *Micromachines* **11**(1), 84 (2020)
22. W. Li, C. Zhang, W. Gao, M. Zhou, Neural network self-tuning control for a piezoelectric actuator. *Sensors* **20**(12), 3342 (2020)
23. Y. Liu, H. Liu, H. Wu, D. Zou, Modelling and compensation of hysteresis in piezoelectric actuators based on Maxwell approach. *Electron. Lett.* **52**(3), 188–190 (2016)
24. W. Wang, F. Han, Z. Chen, R. Wang, C. Wang, K. Lu, J. Wang, B. Ju, Modeling and compensation for asymmetrical and dynamic hysteresis of piezoelectric actuators using a dynamic delay Prandtl–Ishlinskii model. *Micromachines* **12**(1), 92 (2021)
25. J. Lee, M. Jin, N. Kashiri, D.G. Caldwell, N.G. Tsagarakis, Inversion-free force tracking control of piezoelectric actuators using fast finite-time integral terminal sliding-mode. *Mechatronics* **57**, 39–50 (2019)
26. X. Zhao, S. Shen, L. Su, X. Yin, Elman neural network–based identification of rate-dependent hysteresis in piezoelectric actuators. *J. Intell. Mater. Syst. Struct.* **31**(7), 980–989 (2020)

27. C. Yang, N. Verbeek, F. Xia, Y. Wang, K. Youcef-Toumi, Modeling and control of piezoelectric hysteresis: a polynomial-based fractional order disturbance compensation approach. *IEEE Trans. Ind. Electron.* **68**(4), 3348–3358 (2020)
28. Y. Cao, J. Huang, Neural-network-based nonlinear model predictive tracking control of a pneumatic muscle actuator-driven exoskeleton. *IEEE/CAA J. Autom. Sin.* **7**(6), 1478–1488 (2020)
29. S. Xie, J. Ren, Tracking Control Using Recurrent-Neural-Network-Based Inversion Model: A Case Study on a Piezo Actuator, in *IEEE Transactions on Industrial Electronics* (2020)
30. C.J. Lin, P.T. Lin, Particle swarm optimization based feedforward controller for a XY PZT positioning stage. *Mechatronics* **22**(5), 614–628 (2012)
31. J. Oh, D.S. Bernstein, Piecewise linear identification for the rate-independent and rate-dependent Duhem hysteresis models. *IEEE Trans. Autom. Control* **52**(3), 576–582 (2007)
32. G.A. Ortiz, D.A. Alvarez, D. Bedoya-Ruíz, Identification of Bouc–Wen type models using the transitional Markov chain Monte Carlo method. *Comput. Struct.* **146**, 252–269 (2015)
33. G. Wang, K. Zhou, Y. Zhang, Parameter identification of piezoelectric hysteresis model based on improved artificial bee colony algorithm. *Mod. Phys. Lett. B* **32**(11), 1850131 (2018)
34. N.N. Son, C. Van Kien, H.P.H. Anh, Parameters identification of Bouc–Wen hysteresis model for piezoelectric actuators using hybrid adaptive differential evolution and Jaya algorithm. *Eng. Appl. Artif. Intell.* **87**, 103317 (2020)
35. M.A.Z. Raja, I. Ahmad, I. Khan, M.I. Syam, A.M. Wazwaz, Neuro-heuristic computational intelligence for solving nonlinear pantograph systems. *Front. Inf. Technol. Electron. Eng.* **18**(4), 464–484 (2017)
36. B. Sun, Y. Cao, Z. Guo, Z. Yan, S. Wen, Synchronization of discrete-time recurrent neural networks with time-varying delays via quantized sliding mode control. *Appl. Math. Comput.* **375**, 125093 (2020)
37. I. Ahmad et al., Neuro-evolutionary computing paradigm for Painlevé equation-II in nonlinear optics. *Eur. Phys. J. Plus* **133**(5), 184 (2018)
38. A. Siraj-ul-Islam et al., Design of cascade artificial neural networks optimized with the memetic computing paradigm for solving the nonlinear Bratu system. *Eur. Phys. J. Plus* **134**(3), 1–13 (2019)
39. Z. Masood et al., Design of Mexican Hat Wavelet neural networks for solving Bratu type nonlinear systems. *Neurocomputing* **221**, 1–14 (2017)
40. I. Ahmad et al., Novel applications of intelligent computing paradigms for the analysis of nonlinear reactive transport model of the fluid in soft tissues and microvessels. *Neural Comput. Appl.* **31**(12), 9041–9059 (2019)
41. J.A. Khan et al., Design and application of nature inspired computing approach for nonlinear stiff oscillatory problems. *Neural Comput. Appl.* **26**(7), 1763–1780 (2015)
42. M.A.Z. Raja, F.H. Shah, M.I. Syam, Intelligent computing approach to solve the nonlinear Van der Pol system for heartbeat model. *Neural Comput. Appl.* **30**(12), 3651–3675 (2018)
43. A. Mehmood et al., Design of neuro-computing paradigms for nonlinear nanofluidic systems of MHD Jeffery–Hamel flow. *J. Taiwan Inst. Chem. Eng.* **91**, 57–85 (2018)
44. A. Ara et al., Numerical simulation for Jeffery–Hamel flow and heat transfer of micropolar fluid based on differential evolution algorithm. *AIP Adv.* **8**(1), 015201 (2018)
45. M.A.Z. Raja, F.H. Shah, A.A. Khan, N.A. Khan, Design of bio-inspired computational intelligence technique for solving steady thin film flow of Johnson–Segalman fluid on vertical cylinder for drainage problems. *J. Taiwan Inst. Chem. Eng.* **60**, 59–75 (2016)
46. M.A.Z. Raja, J.A. Khan, T. Haroon, Stochastic numerical treatment for thin film flow of third grade fluid using unsupervised neural networks. *J. Taiwan Inst. Chem. Eng.* **48**, 26–39 (2015)
47. M.A.Z. Raja, Solution of the one-dimensional Bratu equation arising in the fuel ignition model using ANN optimised with PSO and SQP. *Connect. Sci.* **26**(3), 195–214 (2014)
48. A. Mehmood et al., Integrated computational intelligent paradigm for nonlinear electric circuit models using neural networks, genetic algorithms and sequential quadratic programming. *Neural Comput. Appl.* **32**(14), 10337–10357 (2020)
49. A. Mehmood et al., Design of nature-inspired heuristic paradigm for systems in nonlinear electrical circuits. *Neural Comput. Appl.* **32**(11), 7121–7137 (2020)
50. Z. Sabir et al., Novel design of Morlet wavelet neural network for solving second order Lane–Emden equation. *Math. Comput. Simul.* **172**, 1–14 (2020)
51. M.A.Z. Raja, U. Farooq, N.I. Chaudhary, A.M. Wazwaz, Stochastic numerical solver for nanofluidic problems containing multi-walled carbon nanotubes. *Appl. Soft Comput.* **38**, 561–586 (2016)
52. M.A.Z. Raja, F.H. Shah, E.S. Alaidarous, M.I. Syam, Design of bio-inspired heuristic technique integrated with interior-point algorithm to analyze the dynamics of heartbeat model. *Appl. Soft Comput.* **52**, 605–629 (2017)

53. M.A.Z. Raja, M.A. Manzar, F.H. Shah, F.H. Shah, Intelligent computing for Mathieu's systems for parameter excitation, vertically driven pendulum and dusty plasma models. *Appl. Soft Comput.* **62**, 359–372 (2018)
54. M. Umar et al., Stochastic numerical technique for solving HIV infection model of CD4+ T cells. *Eur. Phys. J. Plus* **135**(6), 403 (2020)
55. Z. Sabir et al., Neuro-heuristics for nonlinear singular Thomas-Fermi systems. *Appl. Soft Comput.* **65**, 152–169 (2018)
56. F. Faisal et al., A new heuristic computational solver for nonlinear singular Thomas-Fermi system using evolutionary optimized cubic splines. *Eur. Phys. J. Plus* **135**(1), 1–29 (2020)
57. A. Zameer et al., Bio-inspired heuristics for layer thickness optimization in multilayer piezoelectric transducer for broadband structures. *Soft. Comput.* **23**(10), 3449–3463 (2019)
58. A. Zameer et al., Intelligent and robust prediction of short term wind power using genetic programming based ensemble of neural networks. *Energy Convers. Manag.* **134**, 361–372 (2017)
59. A.S. Qureshi, A. Khan, A. Zameer, A. Usman, Wind power prediction using deep neural network based meta regression and transfer learning. *Appl. Soft Comput.* **58**, 742–755 (2017)
60. Z. Choudhry et al., Design of reduced search space strategy based on integration of Nelder-Mead method and pattern search algorithm with application to economic load dispatch problem. *Neural Comput. Appl.* **30**(12), 3693–3705 (2018)
61. A.H. Bukhari et al., Fractional neuro-sequential ARFIMA-LSTM for financial market forecasting. *IEEE Access* **8**, 71326–71338 (2020)
62. A. Ara et al., Wavelets optimization method for evaluation of fractional partial differential equations: an application to financial modelling. *Adv. Differ. Equ.* **2018**(1), 8 (2018)
63. M.A.Z. Raja, M.A. Manzar, R. Samar, An efficient computational intelligence approach for solving fractional order Riccati equations using ANN and SQP. *Appl. Math. Model.* **39**(10–11), 3075–3093 (2015)
64. S. Lodhi et al., Fractional neural network models for nonlinear Riccati systems. *Neural Comput. Appl.* **31**(1), 359–378 (2019)
65. M.A.Z. Raja et al., Design of unsupervised fractional neural network model optimized with interior point algorithm for solving Bagley–Torvik equation. *Math. Comput. Simul.* **132**, 139–158 (2017)
66. R. Bouc, Forced vibrations of mechanical systems with hysteresis, in *Proceedings of the Fourth Conference on Nonlinear Oscillations, Prague (1967)*.
67. A. Mehmood et al., Novel computing paradigms for parameter estimation in Hammerstein controlled auto regressive auto regressive moving average systems. *Appl. Soft Comput.* **80**, 263–284 (2019)
68. J.M. Castellanos-Jaramillo, A. Castellanos-Moreno, A. Corella-Madueño, A finite Hopfield neural network model for the oxygenation of hemoglobin. *Phys. Scr.* **95**(7), 075002 (2020)
69. R.A. Mohamed, Modeling electrical properties of nanofluids using artificial neural network. *Phys. Scr.* **94**(10), 105222 (2019)
70. M. Umar et al., Intelligent computing for numerical treatment of nonlinear prey–predator models. *Appl. Soft Comput.* **80**, 506–524 (2019)
71. I. Jadoon et al., Integrated meta-heuristics finite difference method for the dynamics of nonlinear unipolar electrohydrodynamic pump flow model. *Appl. Soft Comput.* **97**, 106791 (2020)
72. C. Liu, Z. Li, W. Hu, L. Xing, H. Peng, Range and dose verification in proton therapy using proton-induced positron emitters and recurrent neural networks (RNNs). *Phys. Med. Biol.* **64**(17), 175009 (2019)
73. B.J. Wolf, S. Warmelink, S.M. van Netten, Recurrent neural networks for hydrodynamic imaging using a 2D-sensitive artificial lateral line. *Bioinspir. Biomim.* **14**(5), 055001 (2019)